Fast Frequency Sweep Technique for the Efficient Analysis of Dielectric Waveguides

Sergey V. Polstyanko, Romanus Dyczij-Edlinger, *Member, IEEE,* and Jin-Fa Lee, *Member, IEEE*

***Abstract*— This paper describes a new approach to spectral response computations of an arbitrary two-dimensional (2-D) waveguide. This technique is based on the tangential-vector finite-element method (TVFEM) in conjunction with the asymptotic waveform evaluation (AWE) technique. The former is used to obtain modes characteristics for a central frequency, whereas the latter employs an efficient algorithm to compute frequency moments for each mode. These moments are then matched via Padé approximation to a reduced-order rational polynomial, which can be used to interpolate each mode over a frequency band with a high degree of accuracy. Furthermore, the moments computations and subsequent interpolation for a given set of frequency points can be done much more rapidly than just simple simulations for each frequency point.**

***Index Terms*—Approximation methods, dielectric waveguides, electromagnetic propagation, finite-element method, signal analysis.**

I. Introduction

COMPUTER-AIDED numerical analysis has become a necessary tool for designing microwave and optical waveguiding structures such as microstrip lines, optical channel guides, and optical fibers. Different numerical techniques have been presented in the past to solve a wide variety of dielectric waveguide problems [1]–[5]. Among them is the finite-element method (FEM), which is probably the most versatile [3], [6]–[8]. By discretizing the waveguide cross section into a number of triangles and employing the variational technique, the FEM can be used to accurately predict the propagation characteristics of any arbitrary waveguide.

It has been shown by previous researchers that by using the tangential-vector finite-element method (TVFEM), electromagnetic (EM) characteristics of propagating modes in waveguides can be obtained without the occurrence of so-called spurious solutions [9]–[10]. However, these spurious solutions are not completely eliminated, but are reduced to a set of identifiable nonphysical solutions corresponding to the null-space of the generalized eigenmatrix equation. Consequently, they can slow down the convergence of desirable modes during the solution process and cause additional complications. In this paper, an additional set of constraint equations for the generalized eigenmatrix equation is introduced. By using this set of constraint equations, the nonphysical solutions can be completely suppressed and the solution space is limited only to physical modes.

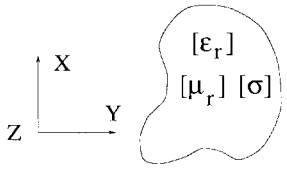

Fig. 1. General anisotropic optical waveguide.

A $\mathcal{H}_0^1(\mathrm{curl})$ TVFEM has been previously implemented to perform a full-wave analysis of an anisotropic waveguide, which is characterized simultaneously by both off-diagonal second-rank symmetric $[\epsilon]$ and $[\mu]$ tensors [11]. However, if one wants to compute a dispersion curve with the propagation constant versus frequency over a given frequency band, this analysis has to be repeated for many sampling frequency points. Consequently, the entire process can become very time consuming, especially when the number of frequency points becomes large and the number of unknowns is significant.

To avoid this difficulty, a new approach based on the asymptotic waveform evaluation (AWE) [12] has been developed. Starting with the known modes' characteristics for a central frequency, the AWE technique employs an efficient algorithm to compute frequency moments for each mode. These moments are then matched via Padé approximation to a reduced order rational polynomial with a high degree of accuracy. Furthermore, the moments computations and subsequent interpolation for a given set of frequency points can be done more rapidly than just simple simulations for each frequency point. To verify the proposed approach, the method has been implemented and tested for sample waveguiding structures and the resultant dispersion curves are compared with those obtained by the $\mathcal{H}_0^1(\mathrm{curl})$ TVFEM. The details of the formulation, error estimation, and sample numerical results will be discussed in the following sections.

II. Formulation

A. Time-Harmonic Maxwell's Equations

In Fig. 1, a general waveguiding structure is shown, which is uniform in the z-direction with an arbitrary cross section Ω in the xy-plane and the boundary of Ω, consisting of either a perfect electric conductor (PEC) or a perfect magnetic conductor (PMC). Assuming time-harmonic excitations, Maxwell's

Manuscript received September 30, 1996; revised January 20, 1997. This work was supported by Hewlett-Packard, Inc.

S. V. Polstyanko and J.-F. Lee are with the ECE Department, Worcester Polytechnic Institute, Worcester, MA 01609 USA.

R. Dyczij-Edlinger is with Motorola Inc., Schaumburg, IL USA.

Publisher Item Identifier S 0018-9480(97)04464-5.

equations can be written as

$$\nabla \times \vec{E} = -j\omega\mu_0[\mu_r]\vec{H}, \qquad \nabla \cdot [\mu_r]\vec{H} = 0$$
$$\nabla \times \vec{H} = j\omega\epsilon_0[\epsilon_r]\vec{E} + [\sigma]\vec{E}, \qquad \nabla \cdot [\epsilon_r]\vec{E} = 0 \tag{1}$$

where $[\epsilon_r]$ and $[\mu_r]$ are the relative permittivity and permeability, respectively, and $[\sigma]$ is the conductivity tensor. In this paper, they are assumed to be diagonal tensors. Furthermore, in the frequency domain, $[\epsilon_r]$ and $[\sigma]$ can be combined to define a complex effective relative permittivity $[\overline{\epsilon_r}]$ as

$$[\overline{\epsilon_r}] = [\epsilon_r] - \frac{j}{\omega\epsilon_0}[\sigma]. \tag{2}$$

To solve for the wave-propagation characteristics, start by expressing the fields as

$$\vec{E}(\vec{r};t) = \vec{\mathcal{E}}(x,y)e^{-\gamma z}e^{j\omega t}$$
$$\vec{H}(\vec{r};t) = \vec{\mathcal{H}}(x,y)e^{-\gamma z}e^{j\omega t} \tag{3}$$

where $\gamma = \alpha + j\beta$ is the propagation constant with α, β being the attenuation and phase constant, respectively, and $\vec{r} = (x,y,z)$ denotes the position vector of a point in the waveguide.

B. A–V Formulation

In the current formulation, a vector potential, $\vec{A}$, and a scalar potential, φ, are used as unknown variables. They are defined through the fields as

$$\vec{B} = \nabla \times \vec{A} \quad \vec{E} = -j\omega\vec{A} - c\nabla\varphi. \tag{4}$$

Also, it is well known that the vector potential $\vec{A}$ defined by (4) is not unique without imposing a gauge condition. Instead of using the conventional Coulomb or Lorenz gauge, $A_z = 0$ is chosen. This condition will greatly simplify the formulation. By using (1)–(4) and the gauge condition $A_z = 0$, Maxwell's equations become

$$\nabla \times [\nu]\nabla \times \vec{A}_\tau - k_0^2[\overline{\epsilon_r}]\vec{A}_\tau + jk_0[\overline{\epsilon_r}]\nabla\varphi = 0$$
$$-jk_0\nabla \cdot [\overline{\epsilon_r}]\vec{A}_\tau - \nabla \cdot [\overline{\epsilon_r}]\nabla\varphi = 0 \tag{5}$$

where $k_0 = \omega^2\epsilon_0\mu_0$ is the free-space wavenumber and $[\nu] = [\mu_r]^{-1}$ denotes the inverse matrix of $[\mu_r]$. Taking into account that $\nabla = \nabla_\tau - \gamma\hat{z}$, (5) can be rewritten as

$$\nabla_\tau \times \mu_{zz}^{-1}\nabla_\tau \times \vec{A}_\tau - \gamma^2[\nu]_\tau\vec{A}_\tau - k_0^2[\overline{\epsilon_r}]_\tau\vec{A}_\tau + jk_0[\overline{\epsilon_r}]_\tau\nabla_\tau\varphi = 0 \tag{6}$$
$$-\gamma\nabla_\tau \cdot [\nu]_\tau\vec{A}_\tau - jk_0\gamma\bar{\epsilon}_{zz}\varphi = 0 \tag{7}$$
$$-jk_0\nabla_\tau \cdot [\overline{\epsilon_r}]_\tau\vec{A}_\tau - \nabla_\tau \cdot [\overline{\epsilon_r}]_\tau\nabla_\tau\varphi - \gamma^2\bar{\epsilon}_{zz}\varphi = 0 \tag{8}$$

where

$$[\overline{\epsilon_r}]_\tau = \begin{bmatrix} \bar{\epsilon}_{xx} & 0 \\ 0 & \bar{\epsilon}_{yy} \end{bmatrix} \quad [\nu]_\tau = \begin{bmatrix} \nu_{yy} & 0 \\ 0 & \nu_{xx} \end{bmatrix}. \tag{9}$$

Equation (7) can be obtained by subtracting (8) from (6). Subsequently, in the current formulation, the focus is on solving (6) and (8) simultaneously. Furthermore, boundary conditions associated with this formulation are

on PEC's	on *PMC's*
$\vec{n} \times \vec{A}_\tau = 0$	$\vec{n} \times ([\nu]\nabla \times \vec{A}_\tau) = 0$
$\varphi = 0$	$[\overline{\epsilon_r}]_\tau(jk_0\vec{A}_\tau + \nabla_\tau\varphi) \cdot \vec{n} = 0$

(10)

where $\vec{n}$ is the normal vector to the boundary.

III. Finite-Element Implementation

A. The Bilinear Form

Equations (6) and (8), and boundary conditions (10) describe a well-defined boundary value problem (BVP) and are ready for the application of the FEM. Application of the Galerkin's method for the current BVP results in the following bilinear form:

$$B(\vec{v},\vec{a}) = \int_\Omega \{\mu_{zz}^{-1}(\nabla_\tau \times \vec{v}_\tau) \cdot (\nabla_\tau \times \vec{a}_\tau) - k_0^2\vec{v}_\tau \cdot [\overline{\epsilon_r}]_\tau\vec{a}_\tau + \nabla_\tau v_z \cdot [\overline{\epsilon_r}]_\tau\nabla_\tau a_z + jk_0\vec{v}_\tau \cdot [\overline{\epsilon_r}]_\tau\nabla_\tau a_z + jk_0\nabla_\tau v_z \cdot [\overline{\epsilon_r}]_\tau\vec{a}_\tau\}d\Omega - \gamma^2\int_\Omega \{\vec{v}_\tau \cdot [\nu]_\tau\vec{a}_\tau + \bar{\epsilon}_{zz}v_z a_z\}d\Omega \tag{11}$$

where $\vec{v},\vec{a}$ are the testing and trial fields, respectively. Notice that in an effort to balance the smoothness requirements on both the trial and testing fields, Green's theorems are adopted to derive (11). Moreover, to facilitate this paper's discussion, a vector notation has been employed for the potentials as

$$\vec{a} = \begin{bmatrix} \vec{a}_\tau \\ a_z \end{bmatrix} = \begin{bmatrix} \vec{A}_\tau \\ \varphi \end{bmatrix}. \tag{12}$$

Judging from the bilinear form (11), a vector field $\vec{a}$ is admissible in the bilinear form if, and only if,

$$\vec{a} \in V = \{\vec{v}:\ \vec{v}_\tau \in (L_2(\Omega))^2, \qquad \nabla_\tau \times \vec{v}_\tau \cdot \hat{z} \in L_2(\Omega), \quad v_z \in C^0(\Omega)\} \tag{13}$$

where $L_2(\Omega)$, $C^0(\Omega)$ are the sets of square integrable functions and continuous functions in Ω, respectively.

B. Two-Dimensional (2-D) $\mathcal{H}_0^1(\mathrm{curl})$ TVFEM

In the Galerkin's process, one needs to find a complex number γ and a vector function $\vec{a} \in V$, such that $B(\vec{v},\vec{a}) = 0$ for every $\vec{v}$ in the infinite dimensional space V. The FEM is nothing but replacing V by a sequence of finite dimensional subspaces V^h contained in V. In the present approach, V^h has been chosen to be spanned by the $\mathcal{H}_0^1(\mathrm{curl})$ TVFEM basis functions. Mathematically, a finite dimensional vector space is defined as $\mathcal{H}^k(\mathrm{curl};\Omega^h)$, for a 2-D discretization Ω^h as

$$\mathcal{H}^k(\mathrm{curl};\Omega^h) = (P_k(\Omega^h))^2 \oplus S_{k+1}(\Omega^h) \tag{14}$$

where $P_k(\Omega^h)$ is the set of piecewise polynomials in Ω^h with order complete to k. The function space $S_{k+1}(\Omega^h)$ can be defined simply by

$$S_k(\Omega^h) = \{\vec{v}_\tau^h \mid \vec{v}_\tau^h \in (\tilde{P}_k(\Omega^h))^2,\ \langle\vec{v}_\tau^h, \nabla_\tau\phi^h\rangle = 0, \ \forall\phi \in \tilde{P}_{k+1}(\Omega^h)\} \tag{15}$$

and $\tilde{P}_k(\Omega^h)$ is the set of piecewise homogeneous kth order polynomials in Ω^h. The function space $\mathcal{H}_0^k(\mathrm{curl};\Omega^h)$ is further defined by

$$\mathcal{H}_0^k(\mathrm{curl};\Omega^h) = \{\vec{v}_\tau^h \mid \vec{v}_\tau^h \in \mathcal{H}^k(\mathrm{curl};\Omega^h), \ \hat{n} \times \vec{v}_\tau^h = 0 \text{ on } \Gamma_{\mathrm{PEC}}\}. \tag{16}$$

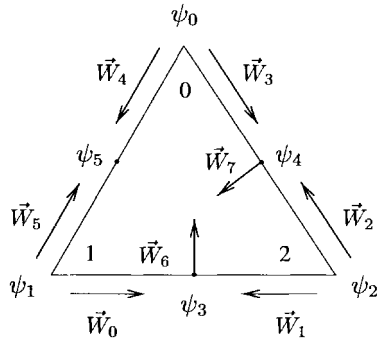

Fig. 2. 2-D $\mathcal{H}_0^1(\mathrm{curl})$ tangential vector element.

Henceforth, the finite dimensional space V^h that is used in the current FEM formulation is

$$V^h = \{\vec{v}^h \mid \vec{v}_\tau^{\,h} \in \mathcal{H}_0^1(\mathrm{curl};\Omega^h),\ v_z^h \in P_2(\Omega^h),\ v_z^h = 0 \text{ on } \Gamma_{\mathrm{PEC}}\}. \tag{17}$$

Note that in choosing the FEM space as in (17), the following statement is valid: $\forall \vec{v}^h \in V^h$; thus, we have $\nabla v_z^h \in \mathcal{H}_0^1(\mathrm{curl};\Omega^h)$. Explicitly, for a triangular element there are eight vector-basis functions and six scalar-basis functions for the finite-element space V^h (Fig. 2). Each trial/testing function $\vec{a}^h \in V^h$ can now be written as

$$\vec{a}_\tau^{\,h} = \sum_{i=0}^{7} a_{\tau i}^h \vec{W}_i^h, \qquad a_z^h = \sum_{i=0}^{5} a_{zi}^h \psi_i^h \tag{18}$$

where the six scalar-basis functions ψ_i are the usual second-order FEM basis functions, namely

$$\begin{aligned}
\psi_0 &= 2\xi_0(\xi_0 - 1/2)\\
\psi_1 &= 2\xi_1(\xi_1 - 1/2)\\
\psi_2 &= 2\xi_2(\xi_2 - 1/2)\\
\psi_3 &= 4\xi_1\xi_2\\
\psi_4 &= 4\xi_0\xi_2\\
\psi_5 &= 4\xi_0\xi_1
\end{aligned}$$

and the eight vector basis functions are given by

$$\begin{aligned}
\vec{W}_0 &= \xi_1\nabla\xi_2 - \xi_2\nabla\xi_1\\
\vec{W}_1 &= \xi_1\nabla\xi_2 + \xi_2\nabla\xi_1\\
\vec{W}_2 &= \xi_2\nabla\xi_0 - \xi_0\nabla\xi_2\\
\vec{W}_3 &= \xi_2\nabla\xi_0 + \xi_0\nabla\xi_2\\
\vec{W}_4 &= \xi_0\nabla\xi_1 - \xi_1\nabla\xi_0\\
\vec{W}_5 &= \xi_0\nabla\xi_1 + \xi_1\nabla\xi_0\\
\vec{W}_6 &= 4\xi_1(\xi_2\nabla\xi_0 - \xi_0\nabla\xi_2)\\
\vec{W}_7 &= 4\xi_2(\xi_0\nabla\xi_1 - \xi_1\nabla\xi_0)
\end{aligned}$$

where ξ_i is the Lagrangian interpolation polynomial or simplex coordinate at vertex i [13].

C. Generalized Eigenmatrix Equation

A generalized eigenmatrix equation can finally be obtained by setting $B(\vec{v},\vec{a}) = 0$ for every $\vec{v}^h \in V^h$. The result is

$$\sum_{\Omega_e}\left(\begin{bmatrix}[A]_e & [C]_e\\ [C]_e^T & [D]_e\end{bmatrix}\right)\begin{bmatrix}\underline{a}_\tau\\ \underline{a}_z\end{bmatrix} = \gamma^2\sum_{\Omega_e}\left(\begin{bmatrix}[B]_e & 0\\ 0 & [E]_e\end{bmatrix}\right)\begin{bmatrix}\underline{a}_\tau\\ \underline{a}_z\end{bmatrix} \tag{19}$$

where $\sum_{\Omega_e}$ means the summation over the contributions from each element and $\underline{a}_\tau, \underline{a}_z$ are the corresponding coefficient vector for the finite dimensional approximation of $\vec{a}^h$. Moreover, the element matrixes in (19) are given by

$$\begin{aligned}
[A]_e &= \int_{\Omega_e}\{\mu_{zz}^{-1}(\nabla_\tau\times\vec{W}_i)\cdot(\nabla_\tau\times\vec{W}_j) - k_0^2\vec{W}_i\cdot[\overline{\epsilon_r}]_\tau\vec{W}_j\}d\Omega\\
[B]_e &= \int_{\Omega_e}\{\vec{W}_i\cdot[\nu]_\tau\vec{W}_j\}d\Omega\\
[C]_e &= jk_0\int_{\Omega_e}\{\vec{W}_i\cdot[\overline{\epsilon_r}]_\tau\nabla_\tau\psi_j\}d\Omega\\
[D]_e &= \int_{\Omega_e}\{\nabla_\tau\psi_i\cdot[\overline{\epsilon_r}]_\tau\nabla_\tau\psi_j\}d\Omega\\
[E]_e &= \int_{\Omega_e}\{\overline{\epsilon}_{zz}\psi_i\psi_j\}d\Omega.
\end{aligned} \tag{20}$$

The integrations in (20) are performed on triangular regions. To make the computation faster, the matrix equation (19) is rearranged as

$$\begin{bmatrix}[B] & 0\\ 0 & [E]\end{bmatrix}\begin{bmatrix}\underline{a}_\tau\\ \underline{a}_z\end{bmatrix} = \frac{1}{\gamma^2+\theta^2}\left(\begin{bmatrix}[A] & [C]\\ [C]^t & [D]\end{bmatrix} + \theta^2\begin{bmatrix}[B] & 0\\ 0 & [E]\end{bmatrix}\right)\begin{bmatrix}\underline{a}_\tau\\ \underline{a}_z\end{bmatrix} \tag{21}$$

where $[A] = \sum_{\Omega_e}[A]_e$ and so on, and $\theta^2 = k_0^2\cdot\mu_{\max}\cdot\epsilon_{\max}$ is an educated guess, which can be obtained by a quasi-TEM approximation for an isotropic medium. The reason for this transformation is as follows. In a lossless dielectric waveguide, a more dominant mode corresponds to a smaller γ^2 value and as a result, the $1/(\gamma^2+\theta^2)$ ratio will be larger. It turns out that although the Lanczos algorithm can compute both the smallest and the largest eigenvalues, the latter almost always converges faster than the former one. Furthermore, from (20) and (21), it can be concluded that for an anisotropic waveguide characterized by diagonal permittivity and permeability tensors, the generalized eigenmatrix equation involves two complex, but symmetric, matrixes. Subsequently, savings in computational time and storage can be realized by taking advantage of this symmetry.

D. Constraint Equations

The eigenpair solutions $\langle\gamma_i,\vec{a}^i\rangle$ to (21) can be divided into three groups as follows. The bilinear form (11) and, subsequently, the generalized eigenmatrix (21) are derived based on (6) and (8). The solutions of (6) and (8) are guaranteed to be nontrivial solutions of Maxwell's equations only if $\gamma \neq 0$. When $\gamma = 0$, there are two possibilities: the cutoff modes, which are still solutions of Maxwell's equations, and the trivial solutions $\vec{a} = \begin{bmatrix}\vec{A}_\tau\\ \varphi\end{bmatrix} \neq 0$, but $\vec{E} = -j\omega\vec{A}_\tau - c\nabla\varphi = 0$. To summarize, the eigenpairs $\langle\gamma_i,\vec{a}^i\rangle$ can be divided into three groups

group 1 (physical modes):
$$\gamma_i \neq 0, \quad \vec{E}_i = -j\omega\vec{A}_\tau^i - c\nabla\varphi^i \neq 0$$
group 2 (cutoff modes):
$$\gamma_i = 0, \quad \vec{E}_i = -j\omega\vec{A}_\tau^i - c\nabla\varphi^i \neq 0$$

group 3 (trivial modes):

$$\gamma_i = 0, \quad \vec{E}_i = -j\omega\vec{A}_\tau^i - c\nabla\varphi^i = 0.$$

This paper's objective is to develop a constrained Lanczos algorithm which will solve for the solutions in group 1 and 2 without the occurrences of group 3. To achieve this goal, one first notices that the group 3 solutions form a vector function space V_{NULL}^h defined as

$$V_{\text{NULL}}^h = \left\{ \begin{bmatrix} \vec{v}_\tau \\ v_z \end{bmatrix} : \ \vec{v}_\tau = Gv_z = \frac{j}{k_0}\nabla_\tau v_z \right\} \tag{22}$$

where G is a gradient operator scaled by the j/k_0 factor, and obviously $V_{\text{NULL}}^h \subset V^h$. Furthermore, the number of trivial modes, or the dimension of V_{NULL}^h, equals the number of free nodes in the second-order discretization. Although these trivial solutions can be easily identified and disregarded at the post-processing stage, their presence can significantly degrade the performance of the Lanczos algorithm. Therefore, a constrained Lanczos algorithm, which completely suppresses the occurrence of these trivial modes, will enhance the numerical efficiency and stability.

E. Orthogonality Relations

From (11), the following orthonormal property exists for the eigensolutions:

$$\int_\Omega \left(\vec{a}_\tau^{\,i} \cdot [\nu]_\tau \vec{a}_\tau^{\,j} + \bar{\epsilon}_{zz} a_z^i a_z^j \right) = \delta_{ij} \tag{23}$$

where δ_{ij} is the Kronecker delta function. Equation (23) is the basis for the constraint equation, which will be used in the constrained Lanczos algorithm. Since a physical solution $\vec{a}^j$ from group 1 or group 2 must be orthogonal to any $\vec{a}^{\,i} \in V_{\text{NULL}}^h$ through (23), the constraint equation for the physical solutions reduces to the following matrix equation:

$$\begin{aligned} &\begin{bmatrix} \underline{v}_z^T G^T & \underline{v}_z^T \end{bmatrix} \begin{bmatrix} [B] & 0 \\ 0 & [E] \end{bmatrix} \begin{bmatrix} \underline{a}_\tau \\ \underline{a}_z \end{bmatrix} = 0 \\ &\Longrightarrow \begin{bmatrix} G^T & I \end{bmatrix} \begin{bmatrix} [B] & 0 \\ 0 & [E] \end{bmatrix} \begin{bmatrix} \underline{a}_\tau \\ \underline{a}_z \end{bmatrix} = 0 \end{aligned} \tag{24}$$

where matrixes $[B]$ and $[E]$ are given by (20). Equation (24) can be used as a set of additional constraints to restrict the solution space to the group 1 and 2 solutions in the Lanczos algorithm.

F. Constrained Lanczos Algorithm

By incorporating the constraint equation (24) into the generalized algorithm, the following algorithm can be used to find N eigenpairs of the generalized eigenmatrix equation $[A]x = \lambda[B]x$ without the occurrences of group 3 solutions:

1) input an initial guess x^0, and set $g^0 = [B]x^0$;
2) orthogonalize g^0
   (a) to previously converged vectors $X_i (i = 1, \cdots n)$: $\tilde{g}^0 = g^0 - \sum_{i=1}^n c_i X_i$, $c_i = X_i^T g^0$;
   (b) to the null space V_{NULL}^h: $\bar{g}_\tau^0 = \tilde{g}_\tau^0$, $\bar{g}_z^0 = -G^T \tilde{g}_\tau^0$;
3) solve $[B]x^1 = \bar{g}_0$ and normalize x^1 to obtain $v_1 = \frac{x^1}{\|x^1\|}$ $(m = 1)$;
4) $f = [A]v_m - h_{m,m}[B]v_m - h_{m-1,m}[B]v_{m-1}$, where
$$h_{m,m} = \frac{v_m^T [A] v_m}{v_m^T [B] v_m}, \qquad h_{m-1,m} = \frac{v_{m-1}^T [A] v_m}{v_{m-1}^T [B] v_{m-1}};$$
5) orthogonalize f
   (a) to previously converged vectors $X_i (i = 1, \cdots n)$: $\tilde{f} = f - \sum_{i=1}^n d_i X_i$, $d_i = X_i^T f$;
   (b) to the null space V_{NULL}^h: $\bar{f}_\tau = \tilde{f}_\tau$, $\bar{f}_z = -G^T \tilde{f}_\tau$;
6) solve for x^{m+1} from $[B]x^{m+1} = \bar{f}$, and set $h_{m+1,m} = \|\bar{x}^{m+1}\|$, $v_{m+1} = \frac{\bar{x}^{m+1}}{\|\bar{x}^{m+1}\|}$;
7) calculate $(\lambda^{(m)}, y^{(m)})$ of the triangular matrix $\mathcal{H}_m$ where
$$\mathcal{H}_m = \begin{bmatrix} h_{1,1} & h_{1,2} & & & & \\ h_{2,1} & h_{2,2} & h_{2,3} & & & \\ & h_{3,2} & h_{3,3} & & & \\ & & & \cdots & & \\ & & & & h_{m,m-1} & h_{m,m} \end{bmatrix}; \tag{25}$$
8) check the residual norm $= h_{m+1,m} |y_m^{(m)}|$ for convergence; if not converged, increment m by 1 and go to step 4;
9) increment n by 1. If all desired modes have converged $(n = N)$ then stop, otherwise go to step 1.

The authors would like to comment here that theoretically, if the initial vector is constructed in such a way that it satisfies (24), their solution becomes orthogonal to the subspace of trivial solutions. The purpose of step 5(b) is simply to avoid the accumulation of a rounding error. Practically, step 5(b) can be performed selectively.

IV. Asymptotic Waveform Evaluation

It has been previously shown that the FEM formulation for the EM wave propagation in 2-D waveguiding structures leads to a matrix equation of the form

$$\mathcal{P}(f)x(f) = \lambda(f)\mathcal{Q}(f)x(f) \tag{26}$$

where $\mathcal{P}(f)$ and $\mathcal{Q}(f)$ are the square complex matrixes, f is a given frequency, x represents the unknown field components, and λ is related to the propagation constant itself. Equation (26) can be solved directly for the unknown eigenpairs $\langle \lambda_i, x_i \rangle$ by using the constrained Lanczos algorithm described above. However, if one is looking for the solution over a given frequency band $[f^0, f^1]$ the entire process has to be repeated for a set of frequencies $\{f_i\}_{i=0}^{i=N}$, such that $f^0 = f_0 < f_1 < \cdots < f_N = f^1$ to find eigenpairs $\langle \lambda_i, x_i \rangle$. After that, the eigenpair $\langle \lambda(f), x(f) \rangle$ for any arbitrary frequency f within the interval $[f^0, f^1]$, can be determined based on an interpolation technique such as linear, quadratic, or spline approximation.

However, if one deals with a big problem, or the number of sampling points N is large, then the entire analysis can become very time consuming. Consequently, this paper's goal is to develop an alternative method for which the spectral responses over a given frequency range can be determined efficiently.

To achieve the above goal, a fast frequency sweep (FFS) technique is proposed and implemented in this paper. The FFS

approach proposed herein is a combination of the TVFEM, described in previous sections, and the AWE technique. The latter has been successfully used for the analysis/simulation of 2-D/three-dimensional (3-D) interconnect structures on integrated circuits and has recently gained much attention from the computer-aided design (CAD) community [12], [14]–[16]. A number of papers have been devoted to AWE as the method for computing an approximation of the response of a linear circuit from the circuit's low-order moments. Furthermore, the method has been proven by many researchers to be an efficient and accurate technique for simulating a lumped linear circuit of arbitrary topologies.

Several attempts have also been recently made to apply the AWE technique for EM problems and the validity of the approach has been shown [17]–[19]. In this paper, the AWE method is extended, based on the rational function approximation for modeling wave propagation in 2-D waveguiding structures. Furthermore, the power series expansion and rational function approximation are compared, and the results of the authors' accuracy are presented.

A. Taylor Expansion

We begin with the following previously obtained generalized eigenmatrix equation:

$$\begin{bmatrix} [A] & [C] \\ [C]^T & [D] \end{bmatrix} \begin{bmatrix} \vec{A}_\tau \\ \varphi_z \end{bmatrix} = \gamma^2 \begin{bmatrix} [B] & 0 \\ 0 & [E] \end{bmatrix} \begin{bmatrix} \vec{A}_\tau \\ \varphi_z \end{bmatrix} \tag{27}$$

where the element matrixes are the same as those given by (20). To facilitate this discussion, (27) is simply rewritten as

$$\mathcal{P}(k)x(k) = \lambda(k)\mathcal{Q}(k)x(k) \tag{28}$$

where matrixes $\mathcal{P}(k)$, $\mathcal{Q}(k)$, and eigenpairs $\langle \lambda(k), x(k) \rangle$ are in general functions of the wavenumber k as follows:

$$\mathcal{P}(k) = \begin{bmatrix} [A] & [C] \\ [C]^T & [D] \end{bmatrix}$$
$$\mathcal{Q}(k) = \begin{bmatrix} [B] & 0 \\ 0 & [E] \end{bmatrix}$$
$$x(k) = \begin{bmatrix} \vec{A}_\tau \\ \varphi_z \end{bmatrix}. \tag{29}$$

These quantities are first expanded by Taylor series around $k = k_0$. Namely,

$$\mathcal{P}(k) = \sum_{i=0}^{N} \mathcal{P}_i (k - k_0)^i$$
$$\mathcal{P}(k) = \sum_{i=0}^{N} \mathcal{P}_i (k - k_0)^i$$
$$\mathcal{Q}(k) = \sum_{i=0}^{N} \mathcal{Q}_i (k - k_0)^i$$
$$\lambda(k) = \sum_{i=0}^{N} \lambda_i (k - k_0)^i$$
$$x(k) = \sum_{i=0}^{N} x_i (k - k_0)^i. \tag{30}$$

Furthermore, from (20), it can be seen that matrix $\mathcal{Q}(k)$ has only the $\mathcal{Q}_0$ component, whereas matrix $\mathcal{P}(k)$ has contributions from $\mathcal{P}_0, \mathcal{P}_1, \mathcal{P}_2$. Substituting (30) into (28) and matching the coefficients of corresponding power of $(k - k_0)$, we end up with the following recursive system of equations to solve:

$$\begin{aligned}
1: \quad & (\mathcal{P}_0 - \lambda_0 \mathcal{Q}_0)x_1 = \mathcal{Q}_0 \lambda_1 x_0 - \mathcal{P}_1 x_0 \\
& \cdots \\
i: \quad & (\mathcal{P}_0 - \lambda_0 \mathcal{Q}_0)x_i = \mathcal{Q}_0(\lambda_i x_0 + \cdots + \lambda_1 x_{i-1}) \\
& \qquad -\mathcal{P}_2 x_{i-2} - \mathcal{P}_1 x_{i-1} \\
& \cdots \\
N: \quad & (\mathcal{P}_0 - \lambda_0 \mathcal{Q}_0)x_N = \mathcal{Q}_0(\lambda_N x_0 + \cdots + \lambda_1 x_{N-1}) \\
& \qquad -\mathcal{P}_2 x_{N-2} - \mathcal{P}_1 x_{N-1}.
\end{aligned} \tag{31}$$

Equation (27) must first be solved for the central frequency f_0 using the constrained Lanczos algorithm described previously. It is worth mentioning that since $\langle \lambda_0, x_0 \rangle$ is an approximate solution to (27), the matrix $\mathcal{P}_0 - \lambda_0 \mathcal{Q}_0$ is nonsingular and can be factorized numerically. Taking into account that x_0 is the eigenvector of (28), and multiplying (31) by x_0^T, λ_i, consequently x_i can be found recursively. Furthermore, in this procedure the orthogonality relation $x_0^T \mathcal{Q}_0 x_i = 0$ must be satisfied for $i > 0$ to insure the numerical stability.

Consequently, in the above process one has to solve the symmetric eigenmatrix equation (27) only once for the central frequency point. After that, the corresponding Taylor series expansion is found by solving (31) with the same matrix $(\mathcal{P}_0 - \lambda_0 \mathcal{Q}_0)$ but different right-hand sides (RHS's). This process can be performed efficiently once the factorization of matrix $(\mathcal{P}_0 - \lambda_0 \mathcal{Q}_0)$ becomes available.

B. Padé Expansion

In many cases, the power-series expansion for the solution of eigenmatrix equation (27) gives fairly good results. However, the situation is different if one wants to find an approximate solution in the proximity of a pole or some other singularity of the desirable function. In such cases, Taylor expansion fails to converge, whereas rational interpolation may still provide satisfactory results. Subsequently, one may want to replace the Taylor expansion by the so-called Padé expansion to improve the accuracy of the numerical solution. In this section, the authors' explain how to construct a rational function for the eigenvalue $\lambda(k)$. The extension of this approach to the eigenvector is straightforward and is not given here. Using the Taylor expansion, one can express an eigenvalue $\lambda(k)$ as

$$\lambda(k) = \sum_{i=0}^{N} \lambda_i (k - k_0)^i \tag{32}$$

whereas in the Padé expansion, one employs a rational polynomial Λ to interpolate $\lambda(k)$ as

$$\Lambda(k) = \left(\sum_{i=0}^{L} p_i (k - k_0)^i \right) \Big/ \left(1 + \sum_{i=1}^{M} q_i (k - k_0)^i \right). \tag{33}$$

The rational function Λ is defined by its $L+M+1$ coefficients (to be determined later). For a given amount of computational

effort, one can usually construct a rational approximation which has a smaller error than a polynomial approximation. Furthermore, for a fixed value of $L+M$, the error is the smallest when $P_L(k)$ and $Q_M(k)$ have the same degree, or $P_L(k)$ has a degree one higher than $Q_M(k)$. The rational polynomial $\Lambda(k)$ is constructed in such a way that it agrees with $\lambda(k)$ at k_0 and their derivative up to $L+M$ degree at $k=k_0$. These conditions result in a system of $L+M+1$ linear equations to solve. Namely

$$\begin{aligned} \lambda_0 - p_0 &= 0 \\ q_1\lambda_0 + \lambda_1 - p_1 &= 0 \\ q_2\lambda_0 + q_1\lambda_1 + \lambda_2 - p_2 &= 0 \\ q_M\lambda_{L-M} + q_{M-1}\lambda_{L-M+1} + \cdots + \lambda_L - p_L &= 0 \end{aligned} \quad (34)$$

and

$$\begin{aligned} q_M\lambda_{L-M+1} + q_{M-1}\lambda_{L-M+2} + \cdots + q_1\lambda_L + \lambda_{L+1} &= 0 \\ q_M\lambda_{L-M+2} + q_{M-1}\lambda_{L-M+3} + \cdots + q_1\lambda_{L+1} + \lambda_{L+2} &= 0 \\ q_M\lambda_L + q_{M-1}\lambda_{L+1} + \cdots + q_1\lambda_{L+M-1} + \lambda_{L+M} &= 0. \end{aligned} \quad (35)$$

The M equations in (35) involve only the unknowns $q_1,\cdots,q_M$ and, thus, must be solved first. Equations in (34) are then used to find $p_0,\cdots,p_L$. Once $q_1,\cdots,q_M$ and $p_0,\cdots,p_L$ are determined, (33) can be used to compute the propagation constant γ at any frequency. The above-described procedure can be repeated to interpolate each component of the eigenvector $x(k)$.

V. Numerical Results

To validate the proposed approach, several examples have been studied. In this paper's first example, the FFS method was applied to a partially filled isotropic waveguide. Then, the method was tested on an anisotropic waveguide. Finally, a shielded microstrip line and a coplanar waveguide were considered. For each example, a dispersion curve with the propagation constant versus frequency has been computed. For all examples, L and M values have been chosen to be equal to 15. The results were compared with the solution obtained by using the TVFEM for different frequency points. Furthermore, to perform an accuracy study of the proposed method over a frequency range, the error is defined by

$$\text{error} = \frac{|\mathcal{P}(k)x(k) - \lambda(k)\mathcal{Q}(k)x(k)|}{|x(k)|} \quad (36)$$

where $\mathcal{P}(k)$, $\mathcal{Q}(k)$ are the exact matrixes from (28) and $\lambda(k)$, $x(k)$ are the approximate solutions. To compare the performance of Taylor and Padé expansions, the error versus frequency for each example have been plotted and comparisons have also been made.

A. Partially Filled Waveguide

To verify the proposed FFS method, a rectangular waveguide partially loaded with a dielectric was first studied, which is a well-known example that has been analyzed by many researchers. For the geometry shown in the inset of Fig. 3, the cutoff frequency of the dominant mode equals 31 MHz. The authors' objective was to demonstrate that the FFS method can correctly predict mode characteristics below the cutoff frequency.

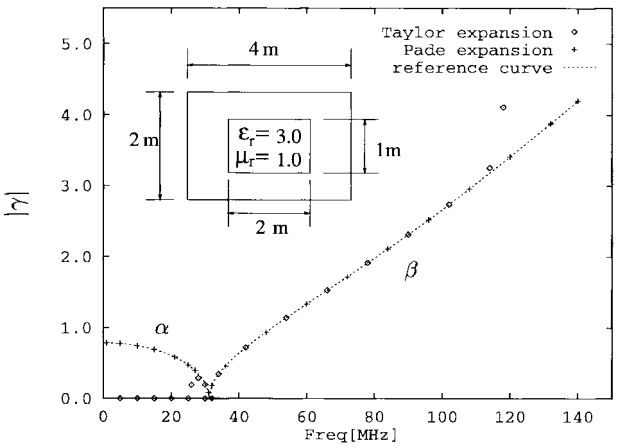

Fig. 3. Dispersion curve of the fundamental mode for the partially filled waveguide. Central frequency has been chosen to be $f_0 = 70$ MHz. Inset shows a dielectric waveguide filled with an isotropic material.

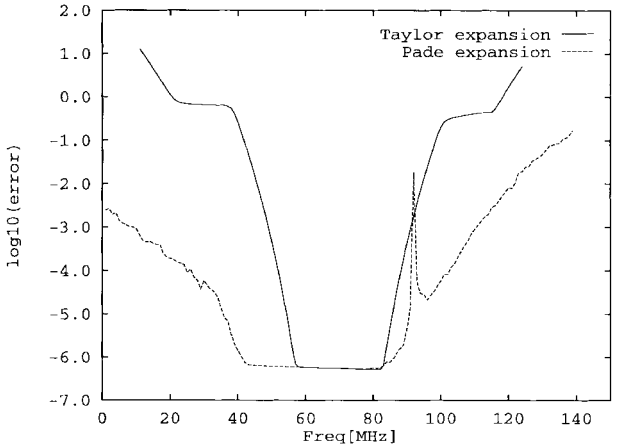

Fig. 4. Error versus frequency for the central frequency $f_0 = 70$ MHz.

The $\mathcal{H}_0^1(\text{curl})$ method is initially used to plot the reference dispersion curve for the dominant mode over the frequency interval from 1 to 140 MHz (Fig. 3). The FFS technique is then applied for the dominant mode starting with the known mode characteristics for $f_0 = 70$ MHz. Two dispersion curves, computed by Taylor and Padé expansions, have been obtained and plotted in Fig. 3 for $f \in$ [1 MHz, 140 MHz]. From Fig. 3, one can conclude that for the frequencies smaller than 31 MHz, the dominant solution becomes an attenuating mode, but still the Padé approximation has a good agreement with the reference curve. On the other hand, the power-series expansion fails for frequencies smaller than the cutoff. Error analysis (see Fig. 4), based on (36), only confirms the above conclusion and suggests that in general, Padé expansion may have a potential advantage over Taylor expansion for physical problems with complex zeros and poles. Furthermore, it is worth mentioning that since $\langle \lambda_0, x_0 \rangle$ is an approximate solution to (27) the error is not exactly 0 at the central frequency.

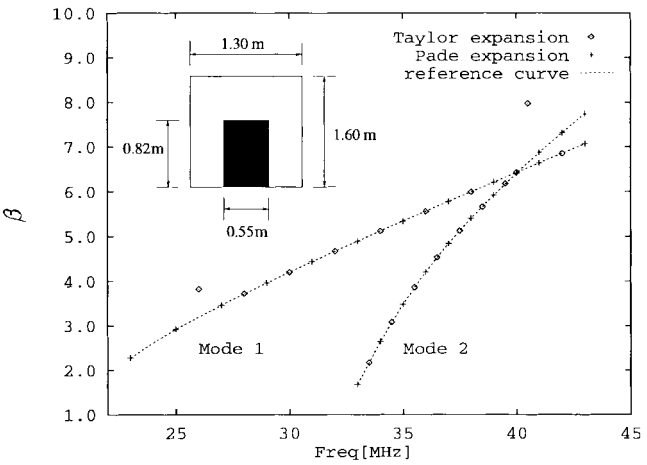

Fig. 5. Dispersion curves for the first two modes of the anisotropic waveguide. Shown in inset is the geometry of the anisotropic dielectric waveguide $\epsilon_{rx} = 170$, $\epsilon_{ry} = \epsilon_{rz} = 85$.

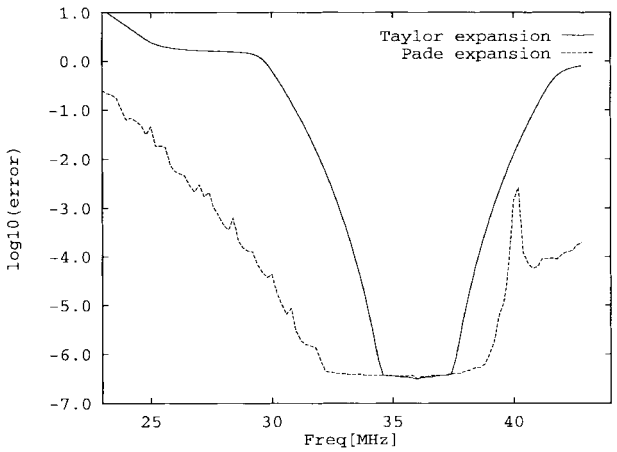

Fig. 6. Error versus frequency for the dominant mode of the anisotropic waveguide for the central frequency $f_0 = 36$ MHz.

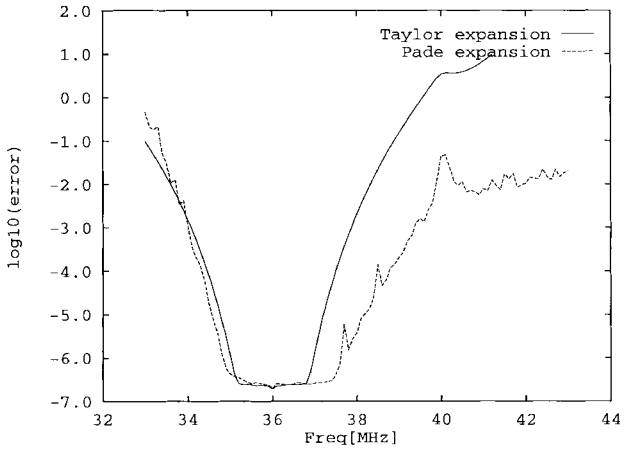

Fig. 7. Error versus frequency for the second mode of the anisotropic waveguide for the central frequency $f_0 = 36$ MHz.

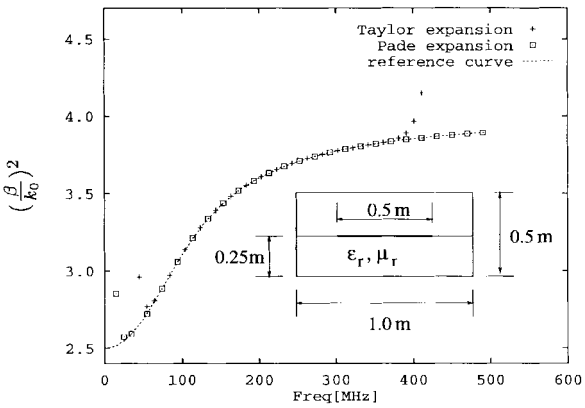

Fig. 8. Dispersion curves for the shielded microstrip line corresponding to the central frequency $f_0 = 200$ MHz. Shown in inset is the geometry of the microstrip line.

B. Anisotropic Waveguide

In this example, a rectangular waveguide is studied, which is loaded with an anisotropic rectangular insert (Fig. 5). The dielectric is made of TiO_2, a material having a very high permittivity $\epsilon_{rx} = 170$ and $\epsilon_{ry} = \epsilon_{rz} = 85$. The interest in this problem arose in connection with the realization of maser amplifiers in the high-frequency region.

The objective for this example was to demonstrate that the FFS technique proposed herein is able to predict multimodes characteristics based on one central frequency point. Reference solutions for this structure have been obtained by using the $\mathcal{H}_0^1(\mathrm{curl})$ TVFEM (Fig. 5). The FFS approach has been applied to the waveguide for the central frequency $f_0 = 36$ MHz, and solutions have been plotted in Fig. 5 and compared with reference results. Furthermore, the error analysis for the first two dominant modes is presented in Figs. 6 and 7, and again, Padé expansion results in a better approximation over the entire frequency range.

C. Shielded Microstrip Line

The next example in this paper is a shielded microstrip transmission line. Fig. 8 shows a sample microstrip line with a strip, which is assumed to be an infinitely thin PEC. The dominant mode, which is used for transmission purposes, is the one having a zero cutoff frequency. At cutoff, it reduces to a transverse electric and magnetic mode.

The solution procedure starts by solving for the normalized propagation constant by using the $\mathcal{H}_0^1(\mathrm{curl})$ TVFEM. After that, the FFS analysis was carried out for the central frequency $f_0 = 200$ MHz. Both Taylor and Padé expansions have been obtained from 1 to 500 MHz, and results are plotted in Fig. 8. The results shown, as well as the error analysis in Fig. 9, prove that the rational polynomial approximation is more accurate than the power series expansion. For example, even though both approaches fail near dc, the Padé expansion agrees very well for high frequencies, whereas the Taylor expansion does not. Moreover, at the lower frequency end, although the Padé expansion fails eventually, its validity extends much further than for the power series expansion.

D. Coplanar Waveguide

Coplanar waveguide (CPW) structures have been attracting considerable attention because of their suitability for broadband microwave integrated circuits (MIC's) and microwave monolithic integrated circuits (MMIC's), as well as the ease of

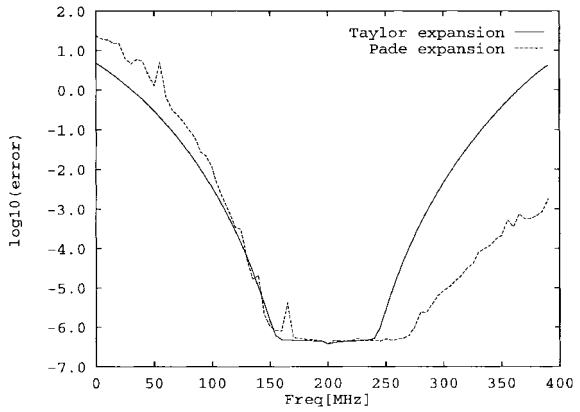

Fig. 9. Error versus frequency for the microstrip line for $f_0 = 200$ MHz.

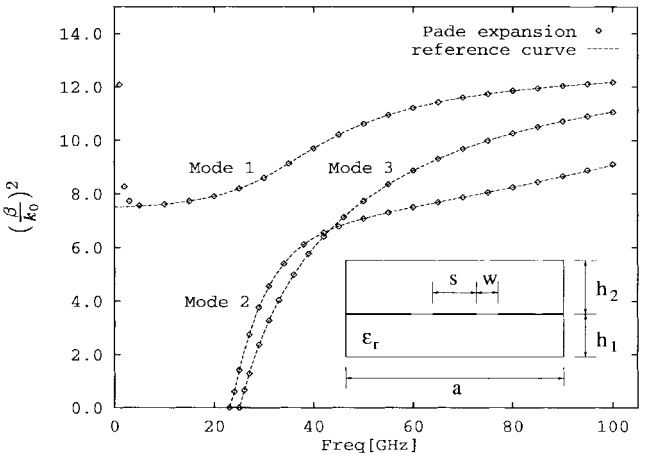

Fig. 10. The dispersion curves for the first three modes for the structure shown in inset with dimensions $w = 0.2$ mm, $a = 2$ mm, $h_1 = 0.2$ mm, $h2 = 0.6$ mm, $s = 0.1$ mm, and $\epsilon_r = 12.9$. Padé expansion has been obtained based on the known modes characteristics for the central frequency $f_0 = 35$ GHz.

incorporation of series and shunt elements. In the final example in this paper, the dispersion characteristics of a conductor-backed coplanar waveguide (CBCPW) in a metal enclosure are studied. The dispersion characteristics are computed for three modes using the proposed FFS procedure.

The structure is enclosed in a perfectly conducting channel and assumed to be uniform and infinite in the z-direction. Both the ground plane and central strips are assumed to be perfectly conducting and infinitely thin, and the dielectric substrate is assumed to be lossless. For this example the comparison between the reference solutions and FFS solutions, for the central frequency $f_0 = 35$ MHz, is presented in Fig. 10. In Fig. 10, only results of the Padé expansion are included, since they are much more accurate than those of the Taylor expansion.

From all examples in this section, it can be concluded, in general, that the FFS procedure provides a good approximation for mode characteristics and may be used in the future for the efficient computations of waveguide modes.

VI. Conclusion

In this paper, the authors have described a novel approach to efficiently compute the spectral responses of arbitrary 2-D waveguides. The proposed technique is based on the TVFEM, in conjunction with the AWE approach. In the FEM computation, the authors have also developed a modified Lanczos algorithm, with an additional set of constraint equations, to completely eliminate nonphysical solutions during the iteration process. This algorithm was combined with the $\mathcal{H}_0^1(\mathrm{curl})$ TVFEM to obtain EM characteristics of propagating modes in waveguides for any given frequency point. The frequency moments for each mode are computed through a recursive procedure to result in a frequency response for a given frequency range. Note that in this recursive procedure, the matrix does not change and only the RHS has to be updated. Thus, the moments calculations become inexpensive when the factorization of the matrix is available. These moments are then matched via Padé approximation to a reduced-order rational polynomial which can be used to interpolate mode over a frequency band with a high degree of accuracy. Numerical results have shown that the $\mathcal{H}_0^1(\mathrm{curl})$ TVFEM, when used together with AWE, provides an efficient procedure for modeling 2-D waveguiding structures.

Acknowledgment

The first author, S. V. Polstyanko, gratefully thanks HPEEsof for the fellowship support of this work.

References

[1] K. S. Kunz and K. M. Lee, "A three-dimensional finite-difference solution of the external response of an aircraft to a complex transient EM environment: Part I—The method and its implementation," *IEEE Trans. Electromag. Compat.*, vol. EMC-20, pp. 328–333, May 1978.

[2] E. Schwig and W. B. Bridges, "Computer analysis of dielectric waveguides: A finite difference method," *IEEE Trans. Microwave Theory Tech.*, vol. MTT-32, pp. 531–541, May 1984.

[3] B. M. A. Rahman and J. B. Davies, "Finite-element analysis of optical and microwave problems," *IEEE Trans. Microwave Theory Tech.*, vol. MTT-32, pp. 20–28, Jan. 1984.

[4] K. S. Yee, "Numerical solution of initial boundary value problems involving Maxwell's equations in isotropic media," *IEEE Trans. Antennas Propagat.*, vol. 14, pp. 302–307, May 1966.

[5] M. D. Feit and J. A. Fleck, "Light propagation in graded-index optical fibers," *Appl. Opt.*, vol. AP-17, pp. 3990–3998, Dec. 1978.

[6] B. Dillon, A. Gibson, and J. Webb, "Cutoff and phase constant of partially filled axially magnetized, gyromagnetic waveguide using finite elements," *IEEE Trans. Microwave Theory Tech.*, vol. 41, pp. 803–807, May 1993.

[7] P. Vandenbulcke and P. E. Lagasse, "Eigenmode analysis of anisotropic optical fibers or integrated optical waveguides," *Electron. Lett.*, vol. 12, no. 5, pp. 120–121, 1976.

[8] J. Lee, D. Sun, and Z. Cendes, "Full-wave analysis of dielectric waveguides using tangential vector finite elements," *IEEE Trans. Microwave Theory Tech.*, vol. 39, pp. 1262–1271, Aug. 1991.

[9] J.-F. Lee, "Finite-element analysis of lossy dielectric waveguide," *IEEE Trans. Microwave Theory Tech.*, vol. 42, pp. 1025–1031, June 1994.

[10] S. H. Wong and Z. J. Cendes, "Combined finite element-modal solution of three-dimensional eddy current problems," *IEEE Trans. Magn.*, vol. 24, pp. 2685–2687, June 1988.

[11] S. V. Polstyanko and J.-F. Lee, "$H_1(\mathrm{curl})$ Tangential vector finite element method for modeling anisotropic optical fibers," *J. Lightwave Technol.*, vol. 13, no. 11, pp. 2290–2295, 1995.

[12] J. E. Bracken, V. Raghvan, and R. A. Rohrer, "Interconnect simulation with asymptotic waveform evaluation," *IEEE Trans. Circuits Syst.*, vol. 39, pp. 869–878, Nov. 1992.

[13] J. Jin, *The Finite Element Method in Electromagnetics*. New York: Wiley, 1993.

[14] R. Kao and M. Horowitz, "Eliminating redundant dc equations for asymptotic waveform evaluation," *IEEE Trans. Computer-Aided Design*, vol. 13, pp. 396–397, Mar. 1994.

[15] S. Kumashiro, R. A. Rohrer, and A. J. Strojwas, "Asymptotic waveform evaluation for transient analysis of 3-d interconnect structures," *IEEE Trans. Computer-Aided Design*, vol. 12, pp. 988–996, July 1993.
[16] L. T. Pillage and R. A. Rohrer, "Asymptotic waveform evaluation for timing analysis," *IEEE Trans. Computer-Aided Design*, vol. 9, pp. 352–366, Apr. 1990.
[17] M. Kuzuoglu, R. Mittra, J. Brauer, and G. Lizalek, "An efficient scheme for finite element analysis in the frequency domain," in *ACES Conf. Proc.*, vol. 2. Monterey, CA, 1996, pp. 1210–1219.
[18] E. K. Miller, "Model-based parameter estimation in electromagnetics: Part II—Applications to EM observables," *ACES Newslett.*, vol. 11, no. 1, pp. 35–56, 1996.
[19] K. Kottapalli, T. K. Sarkar, Y. Hua, E. K. Miller, and G. J. Burke, "Accurate computation of wide-band response of electromagnetic systems utilizing narrow-band information," *IEEE Trans. Microwave Theory Tech.*, vol. 39, pp. 682–687, Apr. 1991.

Sergey V. Polstyanko was born in Moscow, Russia, on November 8, 1973. He received the B.S. degree in electrical engineering from Moscow Engineering Physics Institute, Moscow, Russia, in 1994, and the M.S. degree from Worcester Polytechnic Institute, Worcester, MA, in 1996.

Currently, he is working toward the Ph.D. degree as a Research Assistant in the Department of Electrical and Computer Engineering, Worcester Polytechnic Institute. His research focuses on fast numerical methods for 3-D EM fields computations and EM-field propagation in linear and nonlinear media.

Romanus Dyczij-Edlinger (M'96) was born in Tamsweg, Austria, on June 13, 1966. He received the Dipl.-Ing. and Dr. techn. degrees in electrical engineering from Graz Technical University, Austria, in 1990 and 1994, respectively.

From 1994 to 1995, he was a Post-Doctoral Fellow at Worcester Polytechnic Institute, Worcester, MA. In 1995, he joined Motorola Inc., Schaumburg, IL, where he is currently working on the development of EM simulation tools. His interests include numerical methods in EM.

Jin-Fa Lee (S'85–M'85) was born in Taipei, Taiwan, R.O.C., in 1960. He received the B.S. degree in electrical engineering from National Taiwan University, Taipei, R.O.C., in 1982, and the M.S. and Ph.D. degrees in electrical engineering from Carnegie-Mellon University, Pittsburgh, PA, in 1986 and 1989, respectively.

From 1988 to 1990, he was with ANSOFT Corp., where he developed several CAD/CAE finite-element programs for modeling 3-D microwave and millimeter-wave circuits. From 1990 to 1991, he was a Post-Doctoral Fellow at the University of Illinois, Urbana-Champaign. Currently, he is an Associate Professor in the Department of Electrical and Computer Engineering, Worcester Polytechnic Institute, Worcester, MA. His current research interests are analysis of numerical methods, fast FEM methods, model reduction techniques in computational electromagnetics, 3-D mesh generation, and nonlinear optic-fiber modelings.